Journal of Membrane Science 709 (2024) 123144

Contents lists available at ScienceDirect

Journal of Membrane Science

journal homepage: www.elsevier.com/locate/memsci

3D-/2D-covalent organic framework (COF) bilayered membranes for efficient pharmaceutical purification

Tianci Feng [a], Xiansong Shi [a,**], Tong Ju [a], Jianghai Long [a], Qinghua Liu [a], Ming Liu [a], Yong Wang [a,b,*]

[a] State Key Laboratory of Materials-Oriented Chemical Engineering, College of Chemical Engineering, Nanjing Tech University, Nanjing, 211816, Jiangsu, PR China
[b] School of Energy and Environment, Southeast University, Nanjing, 210096, Jiangsu, PR China

ARTICLE INFO

Keywords:
Covalent organic frameworks
Membrane
Molecular separation
Organic solvent nanofiltration
Pharmaceuticals

ABSTRACT

Covalent organic frameworks (COFs), with their regularly organized structures and solvent resistance, offer distinct advantages for constructing liquid-phase separation membranes. In nearly a decade of development, research has mainly focused on two-dimensional (2D) COFs, which yet give insufficient molecular selectivity due to inherent large pores. Here, we present a mixed-dimensional strategy of growing three-dimensional (3D) COFs on 2D COFs to build bilayered membranes for efficient organic solvent nanofiltration (OSN). The pores of 3D COFs interlace with those of 2D counterparts, resulting in a subnanoporous composite. We develop this 3D-/2D-COFs composite as robust membranes with a nanoscale thickness. The optimal bilayered membrane yields ethanol permeance of 12.2 L m^{-2} h^{-1} bar^{-1} with a molecular weight cutoff as low as ~400 g mol^{-1}, surpassing conventional COF-based OSN membranes. Importantly, the designed 3D-/2D-COFs membrane exhibits stable separation performance and excellent sieving ability to discriminate molecular mixtures. This exceptional molecular selectivity ultimately allows the separation of bioactive pharmaceuticals from impurities through our membrane. Overall, this work provides a design strategy for producing mixed-dimensional COF membranes to advance molecular separation in liquids.

1. Introduction

Traditional separation techniques, such as distillation utilized in petroleum refinement and pharmaceutical engineering, are often characterized by high energy consumption and costs, accounting for up to 50% of their total industrial expenses [1,2]. The transition to energy-efficient and ecofriendly technologies is imperative in the pursuit of global sustainable development. Separation technology based on membranes provides obvious advantages like low energy consumption, ease of operation, and more importantly minimal pollution, making it attractive for separations in recent years [3–5]. With the elaborate design of membrane materials, which are regarded as the core component of membrane processes, membrane technology is available for various challenging separation needs [6,7]. In particular, membrane-enabled nanofiltration in organic liquids, namely organic solvent nanofiltration (OSN), has received great success in the past decade [8]. While conventional polymer membrane materials like polyimide yield promising OSN performance, their inherent limitations, including solvent welling and irregular mass transport channels, hamper long-term use and membrane selectivity [9]. Therefore, there is an urgent need to explore next-generation membrane materials capable of prolonged operation with improved selectivity [10].

Covalent organic frameworks (COFs), known for their long-range ordered structures, represent a new class of crystalline materials with two-dimensional (2D) or three-dimensional (3D) pores [11–13]. Thin films and membranes built of COFs have shown promise in a range of applications including optoelectronic devices and separations [14,15]. Their well-defined channels feature high designability in terms of structure and function, making them attractive for customizing membranes with designed selectivity [16–18]. In addition to desired solvent stability, COFs have been developed as promising building materials to produce high-performance OSN membranes [19–21]. Banerjee and

* Corresponding author. State Key Laboratory of Materials-Oriented Chemical Engineering, College of Chemical Engineering, Nanjing Tech University, Nanjing, 211816, Jiangsu, PR China.
** Corresponding author.
E-mail addresses: xsshi@njtech.edu.cn (X. Shi), yongwang@njtech.edu.cn (Y. Wang).

https://doi.org/10.1016/j.memsci.2024.123144
Received 8 June 2024; Received in revised form 18 July 2024; Accepted 27 July 2024
Available online 29 July 2024

co-workers developed a bottom-up interfacial crystallization strategy to produce COF thin films that achieved fast solvent permeation with decent molecular selectivity [22]. Jiang et al. successfully manipulated the membrane molecular sieving performance using COFs with various alkyl groups [23]. Lai and co-workers developed an interface of ionic liquid and water to generate highly crystalline COF membranes with excellent solvent permeance and rejection of dye molecules [24]. In spite of these achievements, significant challenges remain in the development of COF-based OSN membranes with improved molecular selectivity that could unlock the potential of COFs. Particularly, the existing COF OSN membranes are mostly built of 2D COFs, of which the membrane selectivity barely outperforms that of the traditional membranes due to large pore sizes.

In comparison, 3D COFs often exhibit a cage-like motif with interpenetrated pores, offering smaller mass transport channels that could promote size-dependent selectivity [25,26]. To date, membranes derived from 3D COFs have shown preliminary promise in tackling challenging separation tasks which involve ultrafine species like gases and ions [27,28]. However, the synthesis and control of 3D COF-based membranes present significant challenges, leading to few studies in this area [29,30]. Moreover, the increasing demand for higher separation accuracy necessitates the exploration of COF membranes with predesigned structures. This results in emerging research on structurally tailored COF membranes through topological design and post-synthetic modification [31,32]. In addition, staggered stacking of heterogeneous COFs has proven effective in regulating the size of sieving channels. For instance, Caro and co-workers reported high-performance gas separation membranes based on the bilayered 2D COFs [33]. Zhao et al. developed a multi-interfacial engineering strategy to manipulate the stacking of 2D COFs with specific structures and charges [34]. These pioneering studies provide valuable guidance for preparing advanced COF OSN membranes by virtue of multi-layered structural design.

In this work, we present the design and fabrication of bilayered COF membranes by integrating imine-linked 2D and 3D COFs to enhance molecular selectivity while delivering decent solvent permeance. Utilizing diverse characterization techniques, including gas sorption, X-ray diffraction, and nuclear magnetic resonance spectroscopy, we disclose the intergrowth of crystalline 3D-/2D-COF composites with narrowed pore sizes. The 3D COF is grown on the optimized 2D COF membrane through an interfacial strategy to produce a unique bilayered membrane. This membrane shows superior molecular separation performance *via* nanofiltration dominated by size exclusion, with ethanol permeance of up to 12.2 L m^{-2} h^{-1} bar^{-1} and molecular weight cutoff as low as ~400 g mol^{-1}. Our membrane retains its high performance even after exposure to harsh conditions and 27 days of continuous filtration, underscoring its robust stability. Furthermore, the ultrafine mass transport channels offered by the intergrown 3D-/2D-COF layers facilitate selective sieving of complex solutes. We thereby demonstrate the practical application of the designed 3D-/2D-COF membrane in high-efficient and continuous purification of pharmaceuticals from their precursor compounds. This work leverages the structural diversity and controllability of COFs to engineer high-selectivity OSN membranes which are critically required in industrial separation processes.

2. Experimental section

2.1. Materials

1,3,5-Triformylbenzene (TFB, 99%) and tetra (4-aminophenyl) methane (TAPM, 97%) were supplied by Jilin Chinese Academy of Sciences-Yanshen Technology. Terephthalaldehyde (TPA, 98%), *p*-phenylenediamine (PDA, 97%), *N*,*N*-dimethylformamide (DMF, 99.5%), acetic acid (99.8%), and 1,4-dioxane (99%) were purchased from Aladdin. Mesitylene (97%), 4-nitrophenol (4-NP, 99.5%), vitamin C (99%), curcumin (98%), amoxicillin (99%), tetracycline (98%), rifampicin (RFP, 97%), vitamin B12 (VB-12, 98%), bacitracin (>60 units mg^{-1}), 1-amino-4-methylpiperazine (AMP, 98%), and 5,6-dimethylbenzimidazole (DBI, 99%) were supplied by Macklin. Polyacrylonitrile (PAN, molecular weight (Mw) = 85000 g mol^{-1}) powders and non-woven fabrics were purchased from local vendors. Polyethylene glycol 400 (PEG400, 99.9%) was supplied by Shanghai Lingfeng Chemical Reagent. 1-Butanol (99%), 1-propanol (99.5%), ethanol (EtOH, 99.7%), methanol (MeOH, 99.5%), tetrahydrofuran (THF, 99%), acetone (99.5%), and *n*-hexane (98%) were employed for the evaluation of solvent permeance. Evans blue (EB), Congo red (CR), chrome blue K (CBK), eriochrome black T (EBT), and methyl orange (MO) were supplied by Sinopharm Chemical Reagent. Deionized water (DI water, conductivity = 2–10 μS cm^{-1}) was utilized through this research. All materials were used without additional purification.

2.2. Preparation of porous PAN substrates

A nonsolvent-induced phase separation (NIPS) process was used to prepare PAN substrates. PAN powders (11 g) were vacuum-dried at 80 °C for about 12 h, followed by the addition of PEG400 (4 g, porogen) and DMF (85 g, solvent). The mixture was mechanically stirred at 70 °C for 8 h and subsequently degassed at room temperature for about 24 h to yield a homogeneous solution. The solution was cast onto the non-woven fabric using a 200-μm thick blade and the composite was immersed in DI water for phase inversion. The porous PAN substrates were then stored in DI water prior to further characterization and utilization. The resulting PAN substrate exhibited pure water permeance of ~800 ± 50 L m^{-2} h^{-1} bar^{-1}.

2.3. Synthesis of COF-LZU1, COF-300, and COF-300/COF-LZU1

COF-LZU1 powders were synthesized according to a previously reported method (Fig. S1) [35]. TFB (48 mg, 0.3 mmol), PDA (48 mg, 0.45 mmol), 1,4-dioxane (3.0 mL), and 3 M acetic acid aqueous solution (0.6 mL) were successively added into a Pyrex tube. The prepared precursor solution was ultrasonically treated for 15 min. The tube was flash frozen at 77 K in a liquid N_2 bath and subjected to three freeze-pump-thaw cycles for degassing. After flame sealing, the tube was heated at 120 °C for 72 h, yielding yellow precipitates. The resultant products were washed with 1,4-dioxane and THF through filtration and vacuum-dried at 80 °C overnight to yield COF-LZU1 as a yellow powder. As for the synthesis of COF-300, TPA (12 mg, 0.089 mmol), TAPM (20 mg, 0.052 mmol), 1,4-dioxane (1.0 mL), and 3 M acetic acid aqueous solution (0.2 mL) were added into a Pyrex tube in sequence (Fig. S2) [36]. The rest of the procedures followed that of COF-LZU1. As for the synthesis of COF-300/COF-LZU1 composites, TPA (12 mg, 0.089 mmol), TAPM (20 mg, 0.052 mmol), and COF-LZU1 powders (50 mg) were added into a Pyrex tube, followed by adding 1,4-dioxane (1.0 mL) and 3 M acetic acid aqueous solution (0.2 mL). The rest of the procedures followed that of COF-LZU1.

2.4. Fabrication of COF-300/COF-LZU1 membranes

The COF-300/COF-LZU1 membrane was prepared through secondary growth using a homemade diffusion device (Fig. S3). Here, we synthesized COF-LZU1 as the first layer. TFB (64 mg) and PDA (40 mg) were dissolved in mesitylene (40 mL) and 0.3 M aqueous acetic acid solution (40 mL), respectively. A piece of the PAN substrate was placed between the homemade diffusion device. The prepared organic and aqueous solutions were added simultaneously to both sides of the diffusion device. Next, the device was left undisturbed at room temperature for the specified durations. After the first growth of COF-LZU1, the solutions on both sides of the device were removed, which were washed with mesitylene and DI water, respectively. To prepare the precursor solutions for growing COF-300 on the formed COF-LZU1 membrane, TPA (48 mg) and TAPM (80 mg) were dissolved in mesitylene (40 mL) and 0.6 M aqueous acetic acid solution (40 mL),

respectively. The obtained solutions were added simultaneously to the corresponding sides of the diffusion device. After reaction for 72 h at room temperature in an undisturbed state, the resulting bilayered membrane was thoroughly washed with EtOH and further stored in EtOH before use.

2.5. Filtration tests

OSN performance of the membranes was assessed using a dead-end filtration device with an effective area of ~2 cm^2 under 1 bar. Before testing, the membranes underwent pre-pressing at 1 bar for at least 20 min to achieve a stable condition. The solvent permeation flux (J, L m^{-2} h^{-1}) and permeance (P, L m^{-2} h^{-1} bar^{-1}) of the membranes were calculated as follows:

$$J = V / (A\ \Delta t) \quad (1)$$

$$P = V / (A\ \Delta t\ \Delta p) = J / \Delta p \quad (2)$$

where V (L) is the permeate volume through the effective membrane area A (m^2) under the transmembrane pressure Δp (bar) within the permeation time Δt (h).

Dyes dispersed in water and EtOH, with a concentration of 25 and 20 ppm, respectively, were utilized as the feed to explore molecular separation performance of the membranes. Concentration polarization was minimized by conducting filtration tests under continuous stirring at 350 rpm. The rejection rate (R, %) was calculated as follows:

$$R = (1 - C_p / C_f) \times 100\% \quad (3)$$

where C_p and C_f are the concentrations of the filtration and feed solutions measured by an ultraviolet–visible (UV–vis) spectrophotometer (Thermo Fisher, NanoDrop 2000C). A mixture composed of 20-ppm pharmaceutical and 20-ppm precursor in EtOH was used as the feed to explore the pharmaceutical purification performance of the COF-300/COF-LZU1 membrane. The selectivity (S) was calculated as follows:

$$S = (1 - R_1) / (1 - R_2) \quad (4)$$

where R_1 and R_2 represent the rejection rates of the precursor and the pharmaceutical, respectively.

2.6. Characterizations

Fourier transform infrared spectra (FTIR) data of the monomers, COF powders, and membranes were collected on a Nicolet 8700 spectrometer (Thermo) with the wavenumber ranging from 500 to 4000 cm^{-1}. Particulates and membranes were tested using KBr pressed pellet method and attenuated total reflection (ATR) mode, respectively. ^{13}C solid-state nuclear magnetic resonance (NMR) was taken on a Bruker 400M NMR spectrometer. Powder X-ray diffraction (PXRD) patterns were obtained using a Rigaku SmartLab X-ray diffractometer with a 2-theta range of 2–40° at room temperature. After Au coating, the morphologies of both the powders and membranes were examined using field-emission scanning electron microscopy (SEM, Hitachi S-4800) at an accelerating voltage of 5 kV. Transmission electron microscopy (TEM) was conducted on a JEM-2100F electron microscope at a voltage of 200 kV. N_2 adsorption-desorption measurements of COF powders were carried out at 77 K using a surface area and porosity analyzer (BELSORP MAX). Brunner-Emmett-Teller (BET) surface areas and pore width distributions were determined from the sorption curves based on nonlocal density functional theory (NLDFT). Element analysis was performed using X-ray photoelectron spectroscopy (XPS, Thermo Fisher Scientific, K-alpha). Zeta potentials of the samples were determined using an electrokinetic analyzer (Anton Paar, SurPass 3) through a streaming potential method. The background electrolyte solution was 0.1 mmol L^{-1} KCl solution and the pH value was adjusted by 0.1 M NaOH and HCl solutions. A goniometer (Maist, Dropmeter A100) was used to measure water contact angles of the membranes. Mechanical stability of the COF-300/COF-LZU1 membrane was tested using a nanoindentation system (Bruker, Hysitron TI 980). The COF-300/COF-LZU1 layer together with PAN was exfoliated from the non-woven fabric and vacuum-dried at 120 °C for 24 h before PXRD and N_2 sorption tests.

3. Results and discussion

Membranes derived from conventional 2D COFs often show large effective sieving pores, making them difficult to implement high-selectivity separation in liquids [37]. To resolve this problem, we were dedicated to growing a layer of 3D COFs on top of the original 2D COF membrane. In our case, the extensively studied COF-LZU1 and COF-300 with an identical imine linkage were selected as the representative 2D and 3D COFs, respectively [35,36]. Notably, the chemical robustness offered by COF-LZU1 and COF-300 promises membrane stability, and the high reversibility of the Schiff base reaction to produce imine linkages ensures the intergrowth of the two COFs, preventing gaps or nonselective defects. Fig. 1a illustrates the design of composite membranes on a porous PAN substrate, of which COF-LZU1 is first prepared on the substrate followed by growing the secondary layer of COF-300 to produce a bilayered separation membrane. As the pore size of COF-LZU1 is relatively large, its formation on the PAN substrate will not largely impede the penetration of the COF-300 monomers, thus allowing the growth of COF-300 [38]. As illustrated in Fig. 1b, the addition of COF-300 on top of COF-LZU1 could narrow effective separation channels because of the discrepancy in their framework structures [34]. More importantly, the inherent fine but interconnected pores of COF-300 have the potential to facilitate solvent transport while repelling solutes. Different from the previous studies that leverage laminar structures or charged properties of 2D COFs for gas separation [33,39], we have developed a mixed-dimensional strategy to produce 3D-/2D-COF membranes for molecular separation in liquids. The design of this bilayered heterostructure promises improved molecular selectivity with desired permeation efficiency.

We synthesized COF-LZU1, COF-300, and COF-300/COF-LZU1 composite for structural determinations. FTIR spectra show the attenuation of aldehyde and amine groups from the monomers (Fig. S4), suggesting sufficient consumption in the Schiff-base reaction. In addition, the stretching vibrations at 1621 and 1617 cm^{-1} correspond to the formation of imine linkages for COF-LZU1 and COF-300, respectively. Fig. 2a shows the FTIR spectral results of the COF-300/COF-LZU1 composite and its building units. This spectral result, with the emergence of the stretching vibrations at 1620 cm^{-1}, validates an imine-based structure [40]. More importantly, we observe stretching vibrations at 1700 cm^{-1} in the FTIR spectrum of pristine COF-LZU1 (Fig. S5), suggesting the presence of terminal aldehyde groups. These stretching vibrations from the unreacted aldehyde groups disappear in the FTIR spectrum of the COF-300/COF-LZU1 composite. This indicates that the terminal aldehyde groups potentially serve as active sites to promote covalent bonding between COF-LZU1 and COF-300. The ^{13}C solid-state NMR spectrum in Fig. 2b provides more details into the structural composition of COF-300/COF-LZU1. The signal at ~157 ppm suggests the presence of an imine carbon, matching with its linkage. The observation of the signals at 64 and 191 ppm indicates the characteristic carbons from COF-300 and COF-LZU1, respectively [41,42]. These results confirm that the synthesized solid is composed of COF-LZU1 and COF-300. Analyses of the PXRD patterns reveal that both COF-LZU1 and COF-300 have high crystallinity (Fig. 2c). The diffraction peaks at ~5° and 6.5° in the patterns of COF-LZU1 and COF-300 severally represent their (100) and (200) crystal planes [35,43]. It is worth noting that the COF-300/COF-LZU1 composite exhibits the characteristic diffraction peaks belonging to COF-LZU1 and COF-300, revealing crystalline co-existence.

Next, the morphological examinations through SEM imaging reveal an obvious discrepancy in the microstructures of COF-LZU1 and COF-

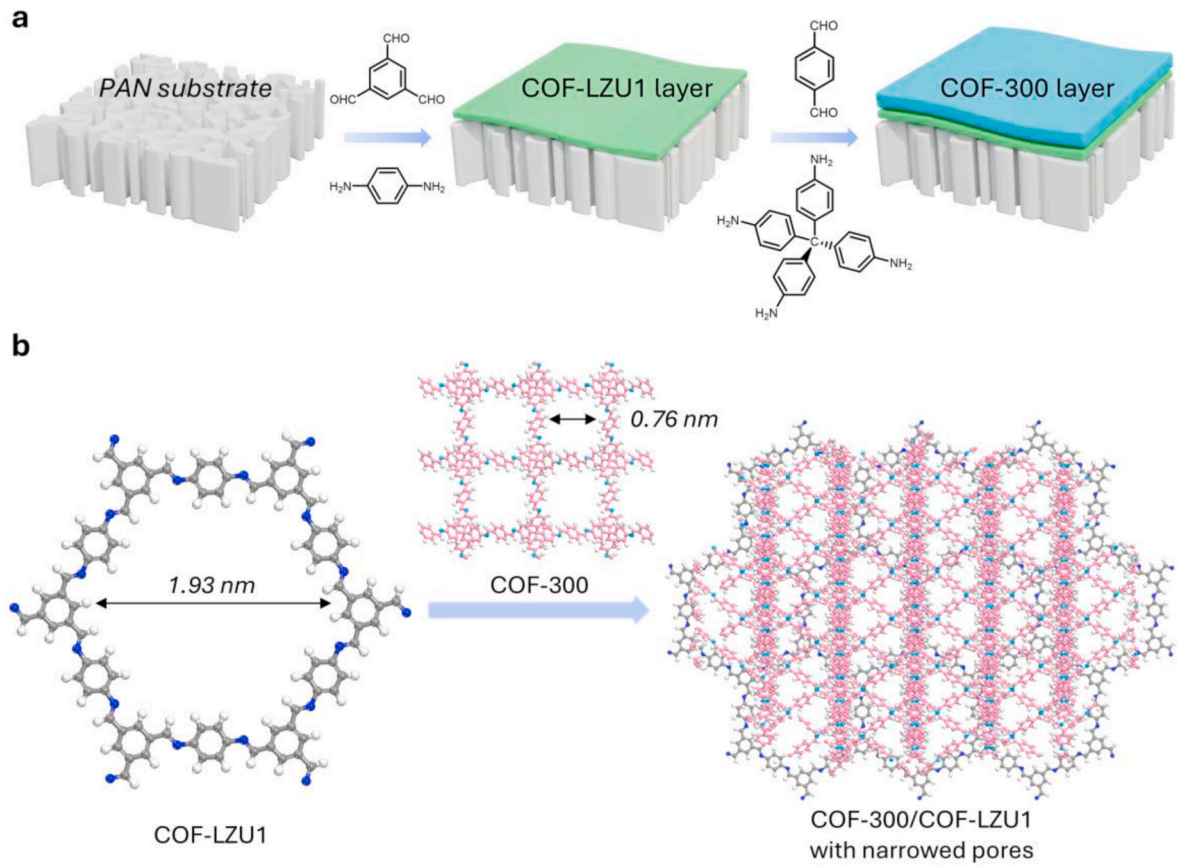

Fig. 1. (a) Schematic diagram for the preparation of COF-300/COF-LZU1 membranes. (b) Schematic diagram of the staggered stacking of COF-LZU1 and COF-300.

300 (Fig. S6). We noticed two kinds of microstructures, *i.e.,* nanoparticles for COF-LZU1 and nanorods for COF-300, in the SEM image of the COF-300/COF-LZU1 composite (Fig. 2d). Besides, the two COFs are tightly grown together thanks to the identical imine linkage with high reversibility [44]. Fig. 2e shows a TEM image of the COF-300/COF-LZU1 composite, which visualizes the intergrowth of the two COFs. 77 K N_2 sorption measurements were performed to explore the pore structure of this intergrown 3D-/2D-COF composite (Fig. 2f). The gas uptake of COF-300/COF-LZU1 composite falls between that of COF-LZU1 and COF-300, consistent with the structural combination. The BET surface areas of COF-LZU1, COF-300, and COF-300/COF-LZU1 are determined to be 304, 1347, and 1069 $m^2\ g^{-1}$, respectively. We applied NLDFT fitting to gain insights into their pore size distributions. The results depicted in Fig. 2g manifest that the pore size distributions of COF-LZU1 and COF-300 are centered at 1.93 and 0.76 nm. In contrast, the pore size of COF-300/COF-LZU1 decreases to 0.63 nm, which stems from the interlaced pore structure [33]. These findings verify the possibility of building fine sieving channels through 3D-/2D-COF composites.

With the success in COF-300/COF-LZU1, we turned to fabricate the corresponding membrane with reduced sieving channels for separation. As revealed by SEM, the growth of COF-LZU1 is dependent on synthesis duration (Fig. S7). Extending the synthesis duration from 24 to 72 h can produce a continuous COF-LZU1 membrane free of noticeable defects (Fig. 3a). Cross-sectional SEM images support incremental growth of COF-LZU1 when the synthesis time prolongs (Fig. S8). With a synthesis duration of 72 h, we obtained a composite membrane with a COF-LZU1 thickness of ~160 nm. The composite membrane surface keeps dense after building COF-300 on top of COF-LZU1 (Fig. 3b). The appearance evolution of these membranes from white through yellow to brown reflects the successive formation of COF-LZU1 and COF-300 (Fig. S9). The cross-sectional SEM image of the COF-300/COF-LZU1 membrane in Fig. 3c reveals a clear increase in thickness from 160 to 410 nm, indicative of COF-300 formation. Furthermore, the reversibility of dynamic imine linkages enables tight intergrowth of COF-300 and COF-LZU1 without obvious gaps. FTIR and XPS tests were used to explore the surface compositions of the resulting composite membranes. Fig. 3d shows the FTIR spectral results of the PAN substrate, COF-LZU1/PAN, and COF-300/COF-LZU1/PAN membranes. The presence of the stretching vibrations at 1625 cm^{-1} referring to imine linkages indicates the growth of COFs. Moreover, the stretching vibrations at 1497 cm^{-1}, which point to C=C bonds, get intensified for the COF-300/COF-LZU1/PAN membrane. This may be related to the significant aromatic backbone of COF-300 [45]. XPS analyses differentiate COF-LZU1 and COF-300 formed on the PAN substrate (Fig. 3e). The notable aromatic backbone of COF-300 generates an increase in the proportion of C=C, while decreasing the hydrophilicity of the composite membrane (Fig. S10). PXRD patterns, along with a N_2 sorption test, further validate the crystalline and microporous structure of the COF-300/COF-LZU1 membrane (Figs. S11–S12). Moreover, Zeta potential tests reveal a negatively charged surface for the prepared composite membranes at a pH range of ~4.1–10 (Fig. 3f), which mainly rises from the electronegativity of carbonyl oxygen in water [46]. The aforesaid results validate the formation of 3D-/2D-COF membranes. We envisage that the proposed strategy could facilitate the systematic construction of mixed-dimensional COF membranes by rationally growing 2D and 3D COFs.

We studied the performance of COF-LZU1 membranes prepared over various durations to optimize the first COF-LZU1 layer. Compared to the neat PAN substrate, which exhibits water permeance of ~800 $L\ m^{-2}\ h^{-1}\ bar^{-1}$ and EBT rejection rate of 5.3% (Fig. S13), the COF-LZU1 membrane synthesized for 24 h performs water permeance of ~86.6 $L\ m^{-2}\ h^{-1}\ bar^{-1}$ and EBT rejection rate of 76.6% (Figs. S14–S15). This sharp contrast validates that the growth of COF-LZU1 effectively improves membrane rejection, though it still adheres to the trade-off between

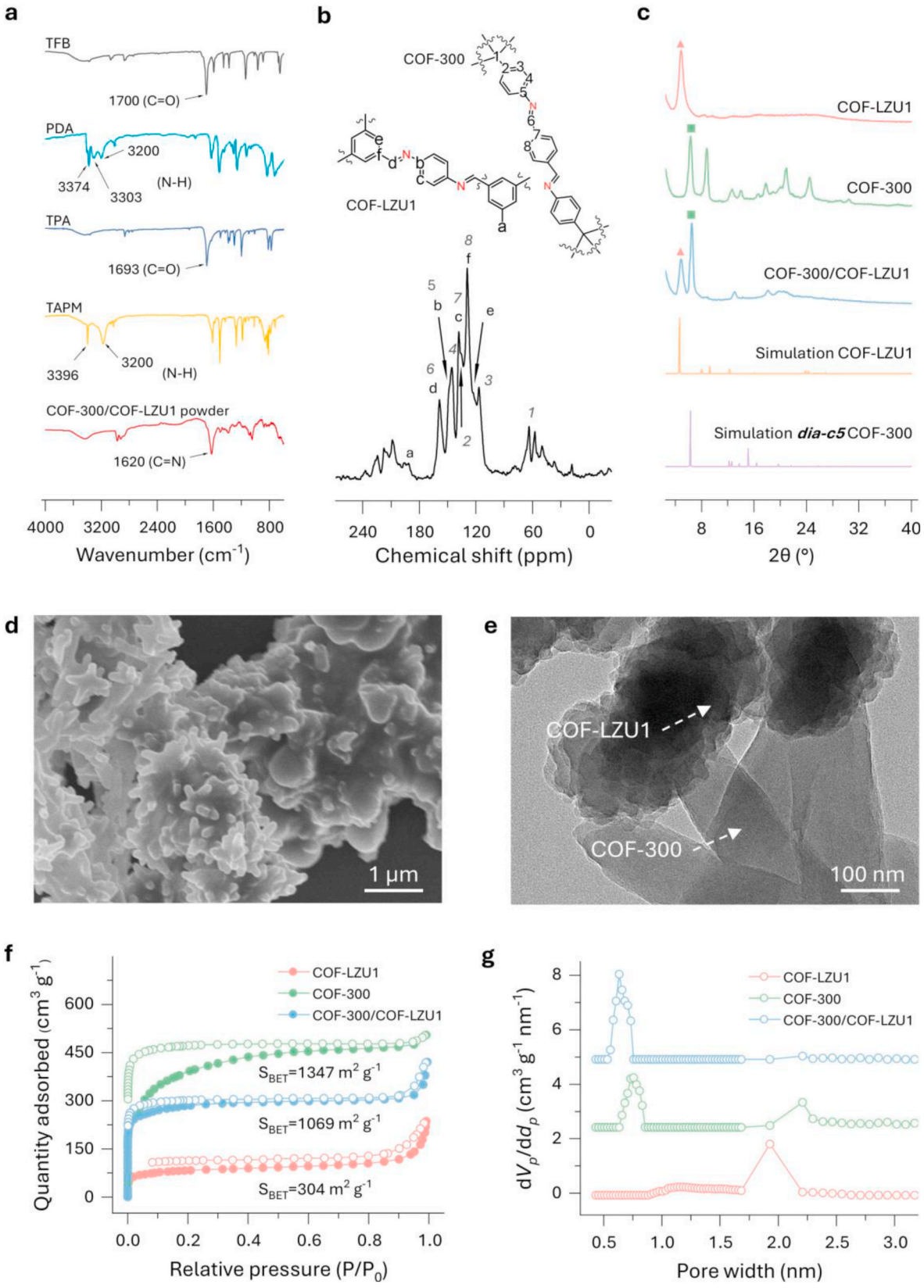

Fig. 2. Characterization of COFs. (a) FTIR spectra of COF-300/COF-LZU1 and its monomers. (b) ^{13}C solid-state NMR spectrum of COF-300/COF-LZU1. (c) Experimental and simulated PXRD patterns of the COFs. (d) SEM and (e) TEM images of COF-300/COF-LZU1. (f) 77 K N_2 adsorption-desorption isotherms of the COF powders and (g) the corresponding pore size distributions.

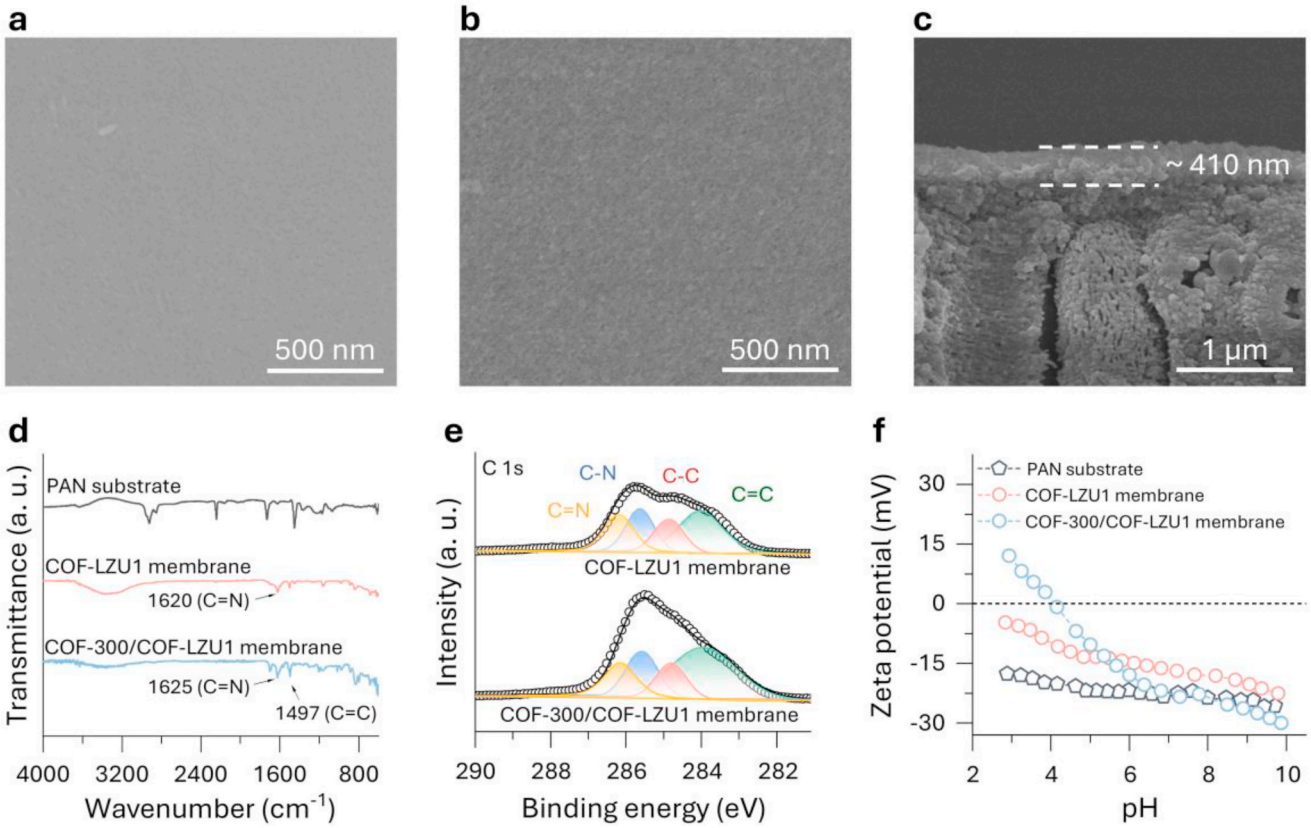

Fig. 3. Characterization of COF-300/COF-LZU1 membranes. (a) Surface SEM image of the COF-LZU1 membrane synthesized for 72 h. (b) Surface and (c) cross-sectional SEM images of the COF-300/COF-LZU1 membrane. (d) FTIR spectra of the substrate and membranes. (e) C 1s XPS spectra of the COF-LZU1 and COF-300/COF-LZU1 membranes. (f) Zeta potential curves of the substrate and membranes.

permeance and selectivity [47]. With a synthesis duration of 72 h, an EBT rejection rate of up to 95.7% together with water permeance of 41.3 L m^{-2} h^{-1} bar^{-1} is achieved by the COF-LZU1 membrane. This membrane was selected as the optimal first layer to grow COF-300 given the balance of permeance and rejection. We then investigated the performance of the bilayered composite membrane. As depicted in Fig. 4a, the building of COF-300 on top of the optimal COF-LZU1 membrane leads to an obvious decrease in solvent permeance, with water and EtOH permeance measured at 21.2 and 12.2 L m^{-2} h^{-1} bar^{-1}. The reduction in solvent permeance mainly originates from two aspects, which are the increased membrane thickness and narrowed channels upon the growth of COF-300. These consequently debase the solvent permeation due to the elevated mass transport resistance [48]. We explored mass transport behaviors in the obtained bilayered COF membrane. Upon plotting the permeances against solvent parameters, including viscosity, Hansen solubility parameter, and kinetic diameter, we found that the solvent permeances exhibit a linear relationship with the reciprocal of their viscosities (Fig. 4b, Fig. S16). This suggests that the solvent transport in our membrane follows the Hagen-Poiseuille equation [49]. To evaluate the impact of the COF-300 growth on selectivity, we tested the molecular rejection rates of both COF-LZU1 and bilayered COF membranes using a range of small molecules (Fig. S17). Fig. 4c presents the molecular rejection curves for these membranes in an aqueous system. The bilayered COF membrane shows higher rejection rates to the probe molecules compared with the COF-LZU1 membrane (Figs. S18–S19). To be specific, the molecular weight cutoff (MWCO) in water decreases from ~460 to ~350 g mol^{-1} upon the addition of COF-300. Given that the membrane surface and these adopted probe molecules are charged, electrostatic interactions in the aqueous environment likely contribute to separation alongside size-dependent exclusion. To determine the effect of pore size on molecular selectivity, we assessed the separation performance of these membranes in EtOH, in which the influence of electrostatic repulsion could be minimized [50–52]. As shown in Fig. 4d, the discrepancy in the selectivity between the two membranes becomes pronounced when the filtration is carried out using EtOH as the solvent. In this case, the COF-LZU1 membrane yields insufficient rejection rates of <90% to all the probe molecules used (Fig. S20). In comparison, the bilayered COF membrane achieves a rejection rate as high as 95.4% for EBT. Its rejection curve gives rise to a low MWCO of ~400 g mol^{-1} (Fig. S21). Given the unchanged crystalline structure of COF-LZU1 upon growing COF-300, this substantial improvement in membrane selectivity likely originates from the narrowed mass transport channels, underscoring the effectiveness of the bilayered COF membrane design. Inspired by the promising membrane performance, we explored its application in separating various bioactive pharmaceuticals and molecules (Fig. S22). The results in Fig. 4e reveal that our bilayered COF membrane can perform high rejections to the targets with molecular weights above 419 g mol^{-1} in EtOH. In particular, the rejection rates for rifampicin (Mw = 822.9 g mol^{-1}), vitamin B12 (Mw = 1355.4 g mol^{-1}), and bacitracin (Mw = 1422.7 g mol^{-1}) reach 94.9%, 96.3%, and 98.1%, respectively (Fig. S23). A summarization of the membrane performance in terms of EtOH and dye MWCO is provided in Fig. 4f, which discloses that our membrane performance is at the forefront of OSN membranes (Table S1).

Membrane robustness determines its potential for practical applications [53,54]. Here, we conducted a range of investigations to assess the physicochemical stability of our bilayered COF membrane. Fig. 5a illustrates the membrane performance against the applied transmembrane pressures. We can observe a nearly linear increase in EtOH permeation flux and relatively stable EtOH permeance when the transmembrane pressure elevates from 1 to 8 bar, indicative of excellent adaptability of the membrane toward pressure variations. Meanwhile,

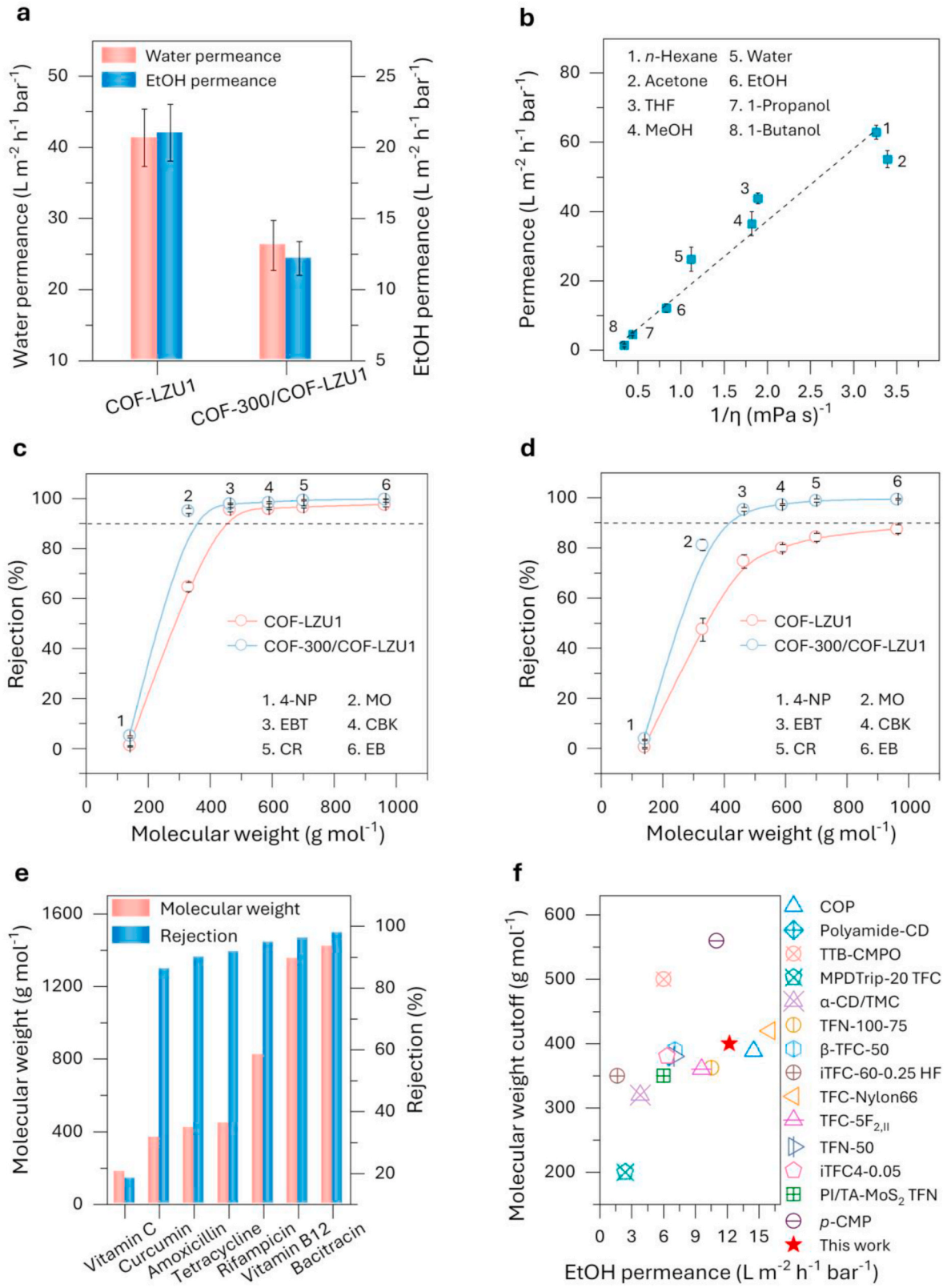

Fig. 4. Performance of COF-300/COF-LZU1 membranes. (a) Water and EtOH permeances of the COF-LZU1 and COF-300/COF-LZU1 membranes. (b) Pure solvent permeance of the COF-300/COF-LZU1 membrane as a function of reciprocal viscosity. (c, d) Molecular rejection curves of the COF-LZU1 and COF-300/COF-LZU1 membranes in water and EtOH. (e) Rejection of the bioactive molecules in EtOH through the COF-300/COF-LZU1 membrane. (f) Performance comparison between the COF-300/COF-LZU1 membrane and others.

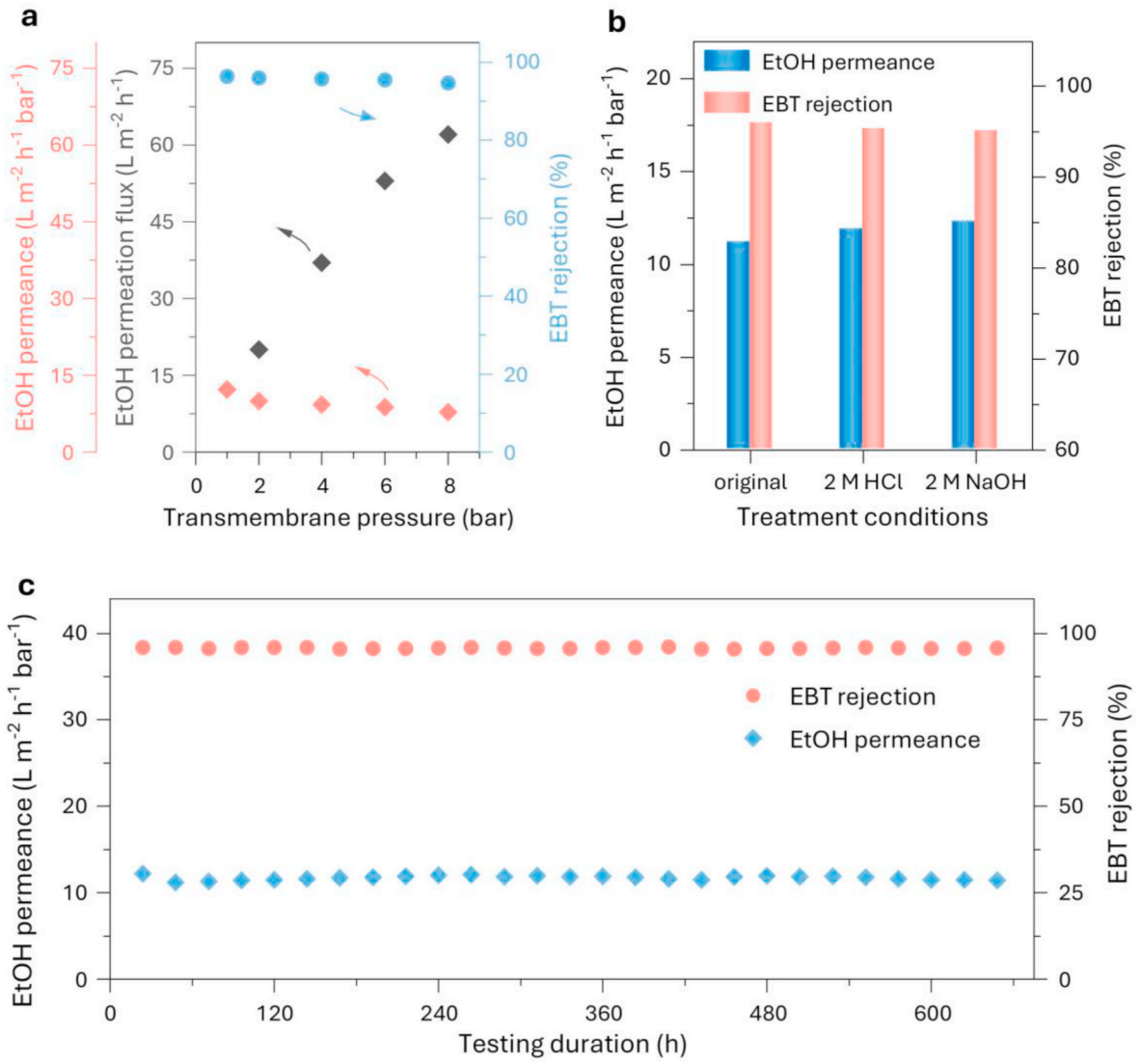

Fig. 5. Stability of the COF-300/COF-LZU1 membrane. (a) Permeance, permeation flux, and EBT rejection in EtOH versus transmembrane pressures. (b) EtOH permeance and EBT rejection before and after treatments. (c) Performance in long-term filtration.

the membrane exhibits negligible change in the EBT rejection at a transmembrane pressure of up to 8 bar, which suggests an intact membrane structure free of damages or breakages. Our membrane demonstrates exceptional resistance to non-neutral testing conditions as well. Both EtOH permeance and EBT rejection keep basically unchanged after being immersed in 2 M HCl and NaOH aqueous solutions for 24 h (Fig. 5b). The membrane supports long-term continuous filtration for 650 h without significant performance degradation (Fig. 5c), revealing its ability to resist potential solvent swelling and decomposition. Moreover, the reduced modulus (*E*) and hardness (*H*) values of the COF-300/COF-LZU1 membrane surface were tested to be 4.84 and 0.26 GPa, respectively (Fig. S24), implying high mechanical robustness [55]. Thus, these tests in terms of elevated pressures, non-neutral conditions, and prolonged operation unambiguously expose the prominent robustness of our membrane.

To highlight the selectivity toward complex mixture, we performed molecular sieving tests using the prepared bilayered COF membrane. Mixed solutes of 4-NP and EBT in EtOH were adopted as the feed to challenge the membrane (Fig. 6a). Notably, the filtrate generated by our membrane is colorless, while the feed solution features a rose-red color (Fig. S25). This visible color change indicates substantial rejection of EBT molecules. UV–vis spectra were employed to confirm the rejection of EBT and the permeation of 4-NP. The results show that the characteristic peak of EBT at ~504 nm disappears and the peak belonging to 4-NP at 310 nm remains prominent, agreeing with effectual solute-solute separation (Fig. 6b). The molecular sieving ability demonstrated above is highly desired in pharmaceutical industries, in which purifying target compounds from their mother solutions is crucial but challenging [56, 57]. We exemplified the selective separation of bioactive RFP and VB-12 from their precursor compounds (Fig. 6c–d, Figs. S26–S27) [58,59]. As shown in Fig. 6e, RFP and its precursor AMP show characteristic peaks at 338 and 207 nm, respectively. These two peaks are present in the spectrum of the prepared mixture, while only the peak referring to AMP remains in the filtrate spectrum. This spectral result demonstrates retention of RFP and passage of AMP, suggesting their effective separation. Similarly, we can notice two peaks at 361 and 287 nm in Fig. 6f, which can be assigned to VB-12 and its precursor DBI, respectively. With the treatment of our membrane, the UV–vis spectrum of the filtrate presents the DBI peak with no trace of VB-12. We quantified the rejection rates of these fine molecules with the results given in Fig. 6g. In these mixed solutions, our membrane retains its high retention rates to concentrate the targeted RFP and VB-12 while allowing free passage of their precursors, as illustrated in Fig. 6h. This capability enabled by our bilayered COF membrane promises simultaneous purification and

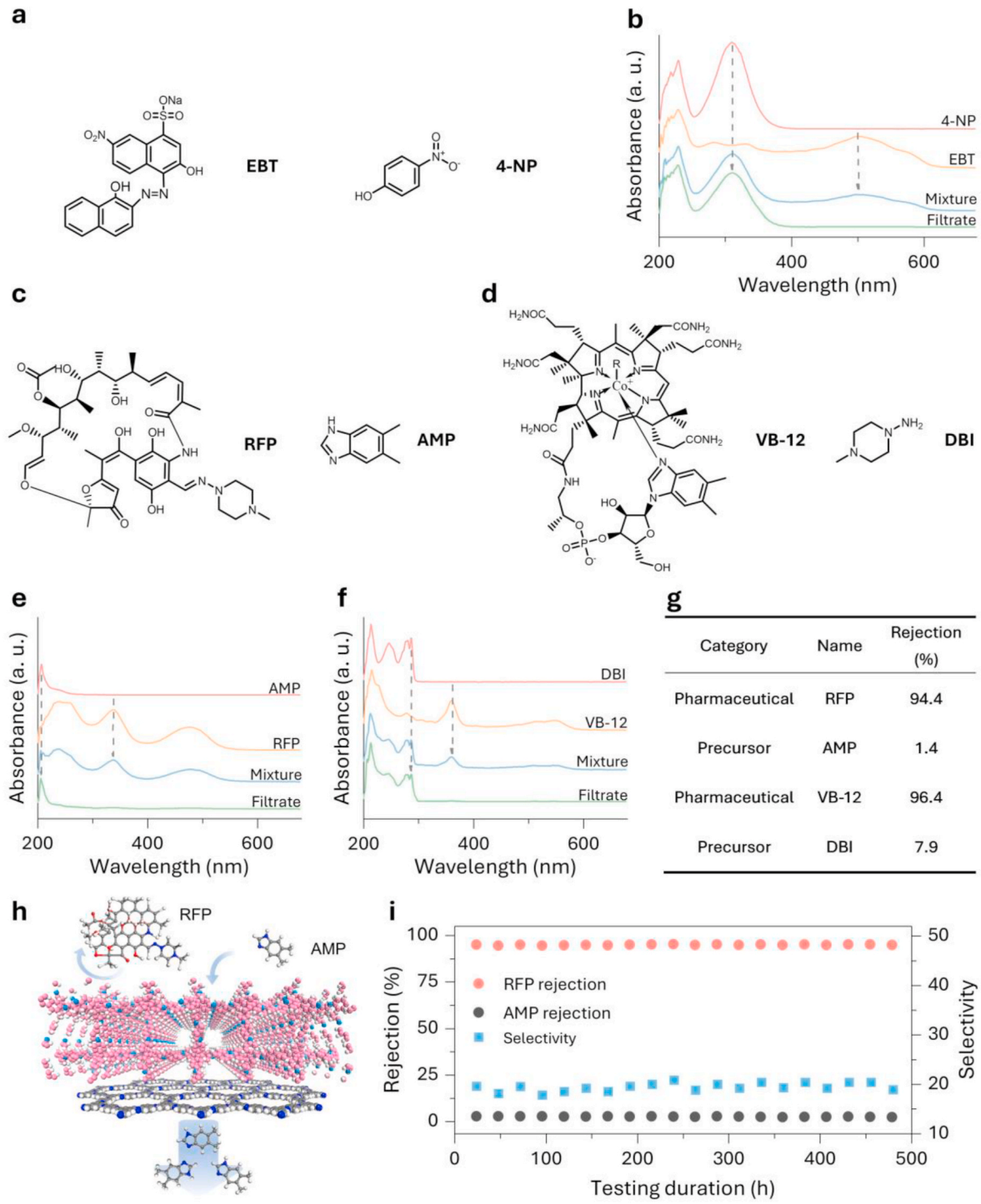

Fig. 6. Molecular sieving and practical application of the COF-300/COF-LZU1 membrane. (a) Molecular structures of the tested molecules. (b) UV–vis spectra for sieving of the EBT/4-NP mixture. (c, d) Molecular structures of the tested drug molecules and their precursors. (e, f) UV–vis spectra for sieving of the RFP/AMP and VB-12/DBI mixtures. (g) Rejection rates of the molecules tested. (h) Schematic diagram of the precise sieving. (i) Long-term sieving of the RFP/AMP mixture.

concentration of pharmaceuticals. To reveal the practicality of our membrane, we conducted a prolonged separation test to discriminate RFP and AMP (Fig. 6i). In continuous operation for 500 h, the RFP and AMP rejection rates keep unchanged, giving stable selectivity as high as ~20. This validates the membrane usability in continuous pharmaceutical purification processes.

4. Conclusions

To conclude, we demonstrate the feasibility of building 3D-/2D-COF composites with narrowed mass transport channels to improve size-dependent molecular selectivity through nanofiltration. The composite, derived from our mixed-dimensional design approach, shows a heterogeneous crystalline structure with a pore size distribution centered at ~0.63 nm. Following this result, we develop COF-LZU1 and COF-300 as the first and secondary selective layers on a porous

substrate, resulting in a robust bilayered composite membrane. Due to the subnanoporous channels, the designed COF-300/COF-LZU1 membrane achieves low molecular weight cutoffs of ~350 and ~400 g mol^{-1} in water and EtOH, with the corresponding solvent permeances of 21.2 and 12.2 L m^{-2} h^{-1} bar^{-1}. This separation performance exceeds that of the conventional membranes composed solely of 2D COFs. In addition, the resulting membrane exhibits excellent stability toward high transmembrane pressures, acid and alkali treatments, and prolonged operation for 650 h. The molecular sieving tests illustrate a pronounced membrane selectivity to achieve accurate solute-solute separation. This prominent selectivity ultimately makes our membrane feasible for purifying and concentrating high-value pharmaceuticals. This work presents a mixed-dimensional strategy leveraging structural diversity of COFs to develop advanced membranes for high-resolution liquid separations.

CRediT authorship contribution statement

Tianci Feng: Writing – review & editing, Writing – original draft, Validation, Investigation, Data curation. **Xiansong Shi:** Writing – review & editing, Writing – original draft, Methodology, Conceptualization. **Tong Ju:** Methodology, Investigation. **Jianghai Long:** Methodology, Investigation. **Qinghua Liu:** Validation, Investigation. **Ming Liu:** Validation, Methodology. **Yong Wang:** Writing – review & editing, Supervision, Funding acquisition, Conceptualization.

Declaration of competing interest

The authors declare that they have no known competing financial interests or personal relationships that could have appeared to influence the work reported in this paper.

Data availability

Data will be made available on request.

Acknowledgments

This work was supported by the National Key Research and Development Program of China (2022YFB3805201) and the National Natural Science Foundation of China (21921006).

Appendix A. Supplementary data

Supplementary data to this article can be found online at https://doi.org/10.1016/j.memsci.2024.123144.

References

[1] C.B. Cunha, M. Brondani, F.D. Mayer, P.P. Lopes, R. Hoffmann, Low-cost small-scale distillation column: assessment of polymeric materials on its economic, chemical, mechanical, and environmental performance, Clean Technol. Environ. Policy 22 (2020) 1547–1563.
[2] T. aus der Beek, F.A. Weber, A. Bergmann, S. Hickmann, I. Ebert, A. Hein, A. Küster, Pharmaceuticals in the environment-global occurrences and perspectives, Environ. Toxicol. Chem. 35 (2016) 823–835.
[3] B. Liang, X. He, J. Hou, L. Li, Z. Tang, Membrane separation in organic liquid: technologies, achievements, and opportunities, Adv. Mater. 31 (2019) 1806090.
[4] Y. Liu, J.H. Dustin Lee, Q. Xia, Y. Ma, Y. Yu, L.Y. Lanry Yung, J. Xie, C.N. Ong, C. D. Vecitis, Z. Zhou, A graphene-based electrochemical filter for water purification, J. Mater. Chem. A 2 (2014) 16554–16562.
[5] R.P. Lively, D.S. Sholl, From water to organics in membrane separations, Nat. Mater. 16 (2017) 276–279.
[6] S. Zhang, S. Zhao, X. Jing, Z. Niu, X. Feng, Covalent organic framework-based membranes for liquid separation, Org. Chem. Front. 8 (2021) 3943–3967.
[7] C. Zhang, B.H. Wu, M.Q. Ma, Z.K. Wang, Z.K. Xu, Ultrathin metal/covalent-organic framework membranes towards ultimate separation, Chem. Soc. Rev. 48 (2019) 3811–3841.
[8] M. Amirilargani, M. Sadrzadeh, E.J.R. Sudhölter, L.C.P.M. de Smet, Surface modification methods of organic solvent nanofiltration membranes, Chem. Eng. J. 289 (2016) 562–582.
[9] J.R. Werber, C.O. Osuji, M. Elimelech, Materials for next-generation desalination and water purification membranes, Nat. Rev. Mater. 1 (2016) 16018.
[10] H. Wang, M. Wang, X. Liang, J. Yuan, H. Yang, S. Wang, Y. Ren, H. Wu, F. Pan, Z. Jiang, Organic molecular sieve membranes for chemical separations, Chem. Soc. Rev. 50 (2021) 5468–5516.
[11] A.P. Cote, A.I. Benin, N.W. Ockwig, M. O'Keeffe, A.J. Matzger, O.M. Yaghi, Porous, crystalline, covalent organic frameworks, Science 310 (2005) 1166–1170.
[12] S. Yuan, X. Li, J. Zhu, G. Zhang, P. Van Puyvelde, B. Van der Bruggen, Covalent organic frameworks for membrane separation, Chem. Soc. Rev. 48 (2019) 2665–2681.
[13] H. Dou, M. Xu, B. Wang, Z. Zhang, G. Wen, Y. Zheng, D. Luo, L. Zhao, A. Yu, L. Zhang, Z. Jiang, Z. Chen, Microporous framework membranes for precise molecule/ion separations, Chem. Soc. Rev. 50 (2021) 986–1029.
[14] S. Bag, H.S. Sasmal, S.P. Chaudhary, K. Dey, D. Blätte, R. Guntermann, Y. Zhang, M. Položij, A. Kuc, A. Shelke, R.K. Vijayaraghavan, T.G. Ajithkumar, S. Bhattacharyya, T. Heine, T. Bein, R. Banerjee, Covalent organic framework thin-film photodetectors from solution-processable porous nanospheres, J. Am. Chem. Soc. 145 (2023) 1649–1659.
[15] K. Dey, S. Kunjattu H, A.M. Chahande, R. Banerjee, Nanoparticle size-fractionation through self-standing porous covalent organic framework films, Angew. Chem. Int. Ed. 59 (2019) 1161–1165.
[16] G. Zhang, M. Tsujimoto, D. Packwood, N.T. Duong, Y. Nishiyama, K. Kadota, S. Kitagawa, S. Horike, Construction of a hierarchical architecture of covalent organic frameworks via a postsynthetic approach, J. Am. Chem. Soc. 140 (2018) 2602–2609.
[17] C. Qian, Q. Qi, G. Jiang, F. Cui, Y. Tian, X. Zhao, Toward covalent organic frameworks bearing three different kinds of pores: the strategy for construction and COF-to-COF transformation via heterogeneous linker exchange, J. Am. Chem. Soc. 139 (2017) 6736–6743.
[18] H. Chen, H.S. Jena, X. Feng, K. Leus, P. van der Voort, Engineering covalent organic frameworks as heterogeneous photocatalysts for organic transformations, Angew. Chem. Int. Ed. 61 (2022) e202204938.
[19] Y. Song, Q. Sun, B. Aguila, S. Ma, Opportunities of covalent organic frameworks for advanced applications, Adv. Sci. 6 (2019) 1801410.
[20] D.B. Shinde, G. Sheng, X. Li, M. Ostwal, A.-H. Emwas, K.-W. Huang, Z. Lai, Crystalline 2D covalent organic framework membranes for high-flux organic solvent nanofiltration, J. Am. Chem. Soc. 140 (2018) 14342–14349.
[21] S. Kandambeth, B.P. Biswal, H.D. Chaudhari, K.C. Rout, S. Kunjattu H, S. Mitra, S. Karak, A. Das, R. Mukherjee, U.K. Kharul, R. Banerjee, Selective molecular sieving in self-standing porous covalent-organic-framework membranes, Adv. Mater. 29 (2017) 1603945.
[22] K. Dey, M. Pal, K.C. Rout, H.S. Kunjattu, A. Das, R. Mukherjee, U.K. Kharul, R. Banerjee, Selective molecular separation by interfacially crystallized covalent organic framework thin films, J. Am. Chem. Soc. 139 (2017) 13083–13091.
[23] E. Zhang, Z. Wu, Q. Wang, Y. Zhao, Y. He, L. Chen, Z. Jiang, Precise and ultra-wide molecular sieving capability with size-dependent COF layers for fast organic solvent nanofiltration, J. Membr. Sci. 692 (2024) 122321.
[24] S. Gao, Z. Li, Y. Yang, Z. Wang, Y. Wang, S. Luo, K. Yao, J. Qiu, H. Wang, L. Cao, Z. Lai, J. Wang, The ionic liquid-H_2O interface: a new platform for the synthesis of highly crystalline and molecular sieving covalent organic framework membranes, ACS Appl. Mater. Interfaces 13 (2021) 36507–36516.
[25] H.M. El-Kaderi, J.R. Hunt, J.L. Mendoza-Cortes, A.P. Cote, R.E. Taylor, M. O'Keeffe, O.M. Yaghi, Designed synthesis of 3D covalent organic frameworks, Science 316 (2007) 268–272.
[26] T. Ma, L. Wei, L. Liang, S. Yin, L. Xu, J. Niu, H. Xue, X. Wang, J. Sun, Y.B. Zhang, W. Wang, Diverse crystal size effects in covalent organic frameworks, Nat. Commun. 11 (2020) 6128.
[27] T. Zhu, Y. Kong, B. Lyu, L. Cao, B. Shi, X. Wang, X. Pang, C. Fan, C. Yang, H. Wu, Z. Jiang, 3D covalent organic framework membrane with fast and selective ion transport, Nat. Commun. 14 (2023) 5926.
[28] Y. Xie, W. Wang, Z. Zhang, J. Li, B. Gui, J. Sun, D. Yuan, C. Wang, Fine-tuning the pore environment of ultramicroporous three-dimensional covalent organic frameworks for efficient one-step ethylene purification, Nat. Commun. 15 (2024) 3008.
[29] X. Shi, Z. Zhang, C. Yin, X. Zhang, J. Long, Z. Zhang, Y. Wang, Design of three-dimensional covalent organic framework membranes for fast and robust organic solvent nanofiltration, Angew. Chem. Int. Ed. 61 (2022) e202207559.
[30] A.K. Mohammed, A.A. Al Khoori, M.A. Addicoat, S. Varghese, I. Othman, M. A. Jaoude, K. Polychronopoulou, M. Baias, M.A. Haija, D. Shetty, Solvent-influenced fragmentations in free-standing three-dimensional covalent organic framework membranes for hydrophobicity switching, Angew. Chem. Int. Ed. 61 (2022) e202200905.
[31] B. Gui, G. Lin, H. Ding, C. Gao, A. Mal, C. Wang, Three-dimensional covalent organic frameworks: from topology design to applications, Acc. Chem. Res. 53 (2020) 2225–2234.
[32] Z. Qu, C. Lai, G. Zhao, A. Knebel, H. Fan, H. Meng, Pore engineering in covalent organic framework membrane for gas separation, Adv. Membr. 2 (2022) 100037.
[33] H. Fan, A. Mundstock, A. Feldhoff, A. Knebel, J. Gu, H. Meng, J. Caro, Covalent organic framework-covalent organic framework bilayer membranes for highly selective gas separation, J. Am. Chem. Soc. 140 (2018) 10094–10098.
[34] Y. Ying, S.B. Peh, H. Yang, Z. Yang, D. Zhao, Ultrathin covalent organic framework membranes via a multi-interfacial engineering strategy for gas separation, Adv. Mater. 34 (2021) 2104946.
[35] S. Ding, J. Gao, Q. Wang, Y. Zhang, W. Song, C. Su, W. Wang, Construction of covalent organic framework for catalysis: Pd/COF-LZU1 in suzuki-miyaura coupling reaction, J. Am. Chem. Soc. 133 (2011) 19816–19822.

[36] F.J. Uribe-Romo, J.R. Hunt, H. Furukawa, C. Klöck, M. O'Keeffe, O.M. Yaghi, A crystalline imine-linked 3-D porous covalent organic framework, J. Am. Chem. Soc. 131 (2009) 4570–4571.
[37] S. Bhunia, K.A. Deo, A.K. Gaharwar, 2D covalent organic frameworks for biomedical applications, Adv. Funct. Mater. 30 (2020) 2002046.
[38] Y. Peng, W.K. Wong, Z. Hu, Y. Cheng, D. Yuan, S.A. Khan, D. Zhao, Room temperature batch and continuous flow synthesis of water-stable covalent organic frameworks (COFs), Chem. Mater. 28 (2016) 5095–5101.
[39] Y.P. Ying, M.M. Tong, S.C. Ning, S.K. Ravi, S.B. Peh, S.C. Tan, S.J. Pennycook, D. Zhao, Ultrathin two-dimensional membranes assembled by ionic covalent organic nanosheets with reduced apertures for gas separation, J. Am. Chem. Soc. 142 (2020) 4472–4480.
[40] C. Qian, L. Feng, W.L. Teo, J. Liu, W. Zhou, D. Wang, Y. Zhao, Imine and imine-derived linkages in two-dimensional covalent organic frameworks, Nat. Rev. Chem 6 (2022) 881–898.
[41] W. Zhao, P. Yan, B. Li, M. Bahri, L. Liu, X. Zhou, R. Clowes, N.D. Browning, Y. Wu, J.W. Ward, A.I. Cooper, Accelerated synthesis and discovery of covalent organic framework photocatalysts for hydrogen peroxide production, J. Am. Chem. Soc. 144 (2022) 9902–9909.
[42] D.M. Fischbach, G. Rhoades, C. Espy, F. Goldberg, B.J. Smith, Controlling the crystalline structure of imine-linked 3D covalent organic frameworks, Chem. Commun. 55 (2019) 3594–3597.
[43] T. Ma, J. Li, J. Niu, L. Zhang, A.S. Etman, C. Lin, D. Shi, P. Chen, L.H. Li, X. Du, J. Sun, W. Wang, Observation of interpenetration isomerism in covalent organic frameworks, J. Am. Chem. Soc. 140 (2018) 6763–6766.
[44] J. Hu, S.K. Gupta, J. Ozdemir, H. Beyzavi, Applications of dynamic covalent chemistry concept toward tailored covalent organic framework nanomaterials: a review, ACS Appl. Nano Mater. 3 (2020) 6239–6269.
[45] S. Li, Y. Yang, H. Shan, J. Zhao, Z. Wang, D. Cai, P. Qin, J. Baeyens, T. Tan, Ultrafast and ultrahigh adsorption of furfural from aqueous solution via covalent organic framework-300, Sep. Purif. Technol. 220 (2019) 283–292.
[46] F. Xu, Y. Wang, C. Lian, Z. Xu, Fast proton-selective transport through covalent organic frameworks in aqueous phase, J. Membr. Sci. 648 (2022) 120361.
[47] H.B. Park, J. Kamcev, L.M. Robeson, M. Elimelech, B.D. Freeman, Maximizing the right stuff: the trade-off between membrane permeability and selectivity, Science 356 (2017) 1138–1148.
[48] Z. Jiang, S. Karan, A.G. Livingston, Water transport through ultrathin polyamide nanofilms used for reverse osmosis, Adv. Mater. 30 (2018) 1705973.
[49] P. Silva, S. Han, A.G. Livingston, Solvent transport in organic solvent nanofiltration membranes, J. Membr. Sci. 262 (2005) 49–59.
[50] X.Y. Wang, J.Y. Yang, X.S. Shi, Z. Zhang, C.C. Yin, Y. Wang, Electrosynthesis of ionic covalent organic frameworks for charge-selective separation of molecules, Small 18 (2022) 2107108.
[51] K.H. Lim, Y. Sun, W.C. Lim, S. Soh, Charging organic liquids by static charge, J. Am. Chem. Soc. 142 (2020) 21004–21016.
[52] P. Marchetti, M.F. Jimenez Solomon, G. Szekely, A.G. Livingston, Molecular separation with organic solvent nanofiltration: a critical review, Chem. Rev. 114 (2014) 10735–10806.
[53] Y. Yao, P. Zhang, F. Sun, W. Zhang, M. Li, G. Sha, L. Teng, X. Wang, M. Huo, R. M. DuChanois, T. Cao, C. Boo, X. Zhang, M. Elimelech, More resilient polyester membranes for high-performance reverse osmosis desalination, Science 384 (2024) 333–338.
[54] K. Suvigya, S. Lalita, K. Gopinadhan, Membranes for desalination and dye separation: are 2D materials better than polymers? a critical comparison, Sep. Purif. Technol. 325 (2023) 124693.
[55] S. Mohata, K. Dey, S. Bhunia, N. Thomas, E.B. Gowd, T.G. Ajithkumar, C.M. Reddy, R. Banerjee, Dual nanomechanics in anisotropic porous covalent organic framework janus-type thin films, J. Am. Chem. Soc. 144 (2022) 400–409.
[56] H. Xiao, Y. Feng, W.R.F. Goundry, S. Karlsson, Organic solvent nanofiltration in pharmaceutical applications, Org. Process Res. Dev. 28 (2024) 891–923.
[57] Y. Cui, T.-S. Chung, Pharmaceutical concentration using organic solvent forward osmosis for solvent recovery, Nat. Commun. 9 (2018) 1426.
[58] S.S. Marwaha, R.P. Sethi, J.F. Kennedy, Role of amino acids, betaine and choline in vitamin B12 biosynthesis by strains of propionibacterium, Enzym. Microb. Technol. 5 (1983) 454–456.
[59] H.G. Floss, T.-W. Yu, Rifamycin-mode of action, resistance, and biosynthesis, Chem. Rev. 105 (2005) 621–632.